A 10 GHz metamaterial sensor to detect SARS COV-2 and dust particles in free space

Massood Tabib-Azar, *Senior Member, IEEE,* Mohammad Ashif Hossain Chowdhury
ECE Department, University of Utah
Salt Lake City, UT 84102

***Abstract*— An X-band, free-space microwave sensor consisting of 30 radial spokes connected in a central hub with a gap region was designed, fabricated and tested. The sensor structure results in an electric dipole at 10 GHz with a split circular disc capacitor at the center. Viruses, dust, and soot particles in the gap region change the sensor's impedance and its reflection coefficient monitored by a horn antenna and a network analyzer. The sensor sensitivity was 85.02 MHz/microliter for deionized water, 89.5 MHz/microliter for uninfected saliva, and 94.6 MHz/microliter for SARS-COV-2 infected saliva with 10^3 viruses/μL. Its sensitivity to a dielectric sample (ε_ρ~5.84) was 3.23 MHz/mm^3, and for iron particles was 16.25 MHz/mm^3. All these samples were smaller than λ/30 at 10 GHz and could not be detected on uniform dielectric or metallic substrates without the spoke structure. A 2x2 array of spoke sensors was also constructed and tested as a feasibility study for designing larger metamaterial (MTM) periodic arrays.**

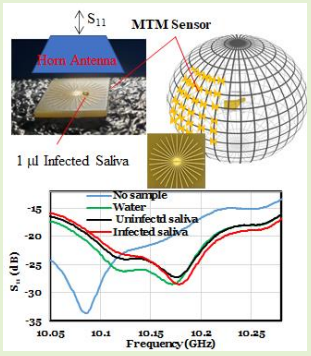

***Index Terms*— Bio Sensing, microwave resonator, SARS-COV-2, dust particle sensing, free space detection, metamaterial, near-field sensors**

I. Introduction

Current SARS-COV-2 pandemic motivated development of sensors to detect airborne viral particles over large areas. Microwave remote sensing techniques have been extensively developed during the past few decades and offer good sensitivity to changes in the impedance of objects interrogated through free space [1]. Respiratory viruses such SARS-COV-2 become airborne and spread through aerosolized particulates generated by coughing or talking. Their detection in air or when they land on available surfaces can provide information necessary to control and prevent their widespread transmission.

The aerosolized exhaled particles are mostly composed of human saliva that may also attract other airborne particles such as soot and dust particle. Healthy person's saliva has an average relative permittivity of 76 [2], while water has a relative permittivity of 78 at room temperature [3] and 80 at 20°C. Human saliva consists of 98-99 % water and 1-2 % of biomarkers, urea, ions, enzymes, and other vital components [4]. Human saliva exhibits different electrical characteristics in the same person depending on her hydration level, fasting, activity level, age and other conditions. Saliva also contains viruses and bacteria in infected individuals. SARS-COV-2 infected individuals can have large load of viruses in their saliva approaching around 10^6/ml. SARS-CoV-2 is a 70-125 nm spherical virus with spiking proteins S1 and S2 [5].

Viruses are composed of capsid proteins and glycoprotein and inner DNA or RNA cores that determine their dielectric properties. Most RNA and DNA viruses have dry relative permittivity of 8-10 [6]. So, when a saliva sample (ε_r~78) is infected with SARS-COV-2 virus, depending on its viral load, it will have slightly lower dielectric constant (ε_{ri}<78) compared to uninfected saliva that can be measured to sense the infected saliva. SARS-CoV-2 viral particles are negatively charged in the saliva leading to slightly higher ionic conductivity.

A real-time (1-5 mins) virus detection system [7-9] can be used to significantly reduce the spread of infection. Large number of rapid sensors are already reported including: saliva-based GO-decorated Au/FBG SARS-COV-2 sensors [10], facile biosensors [10], paper-based electrochemical biosensor [11], nano-materials based biosensors [12,13], colloidal particles and unique interfaces-based SARS-COV-2 detection [14] magnetic Nano-sensor [15], electrochemical saliva sampling [16], rapid electronic SARS-COV-2 sensors [17-19], plasmonic sensors [20-22] etc. There is also a THz sensor which detects spike proteins of the SARS-COV-2 [23]. Most of these sensors require sample preparation and require at least couple of minutes for providing results. If sufficiently developed, the sensors discussed here can detect the virus in shorter times.

To the best of our knowledge the work reported here is the first description of a remote sensing technique capable of detecting SARS-COV-2 viruses residing over large surfaces. It consists of an X-band device with radial spokes connected to a

This work is partially supported by an NSF RAPID Grant, a grant from EXAMIN, LLC and by the USTAR Program. Massood Tabib-Azar is with the ECE Dept. of U of Utah, Salt Lake City, UT 84102 (e-mail address: azar.m@utah.edu). Mohammad Ashif Hossain Chowdhury is with the ECE Dept. of U of Utah, Salt Lake City, UT 84102 (e-mail address: u1368464@utah.edu).

central split hub with a gap region shown in Fig. 1. Spokes at different angles enable the structure to interact with incident electromagnetic waves with different polarizations. One can use these devices in a periodic array to realize a metamaterial (MTM) or meta surfaces with distributed gap regions for distributed sensing of viral and other particles. The spokes form electric dipoles with different polarization angles that produce large electric fields in the gap region when illuminated with an electromagnetic wave. Large fields in the gap makes it an ideal "sensitive" spot for detecting airborne particles. Compared to terahertz waves with very large attenuation in air with humidity, x-band signals have very small attenuation and can be used to remotely interrogate surface sensors from long distances (>100 m). X-band sources and detectors are also far less expensive than terahertz sources and system.

Metamaterials are composite structures that are engineered to exhibit unique electromagnetic properties like negative permittivity and permeability and negative or zero refractive indices [24]. MTMs are also great candidates for sensor applications [25]. In these sensors, the measurand (sensed sample) changes the sensor's resonance and or the amplitude of its reflection/transmission coefficients. In the case of sensors with coupled resonant modes, the measurand changes the strength of their coupling leading to frequency splitting, and to amplitude modulation of a harmonic signal.

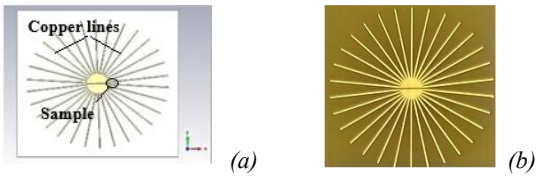

Fig. 1: (a) Geometric Structure of the spoke resonator. (b) Its optical image.

We simulated the sensor's scattering parameters and electric fields using CST microwave studio's Finite Element Method (FEM) frequency domain simulation. The simulation results were then compared with the experimental results that were obtained using an HP 8720C Vector Network Analyzer and Pasternak PE9804WR90 horn antenna. The sensor was tested with deionized water, uninfected saliva, infected saliva, dielectric and metallic samples.

In section II we discuss the MTM sensor structure geometry and simulation results. In section III we present the experimental results for different samples and compare the sensitivity of the MTM sensor with uniform metallic and dielectric substrates as control experiments. Finally, we discuss sensor sensitivity and selectivity and conclude with the summary of results and directions for future studies.

II. Design and Operation Principle

The proposed MTM inspired resonator is shown in Fig.1. It is developed around the idea of an electric dipole structure with many dipoles with varying lengths effectively produced by the angle each spoke makes with the vertically polarized electric field. There are 30 spokes centrally connected to a split hub with a gap. The overall dimension of the structure is 16 mm x 16 mm with a substrate thickness of 1 mm. The 6 mm long, 2 mm wide, vertical spokes on ε_r=4.4 substrate (FR-4) produce a half wavelength dipole at 10 GHz based on our extensive simulations. A 1.1 mm diameter split circular disc at the center provides a 0.004 mm capacitive gap between the upper and lower halves of the structure. The combination of these spokes and the gap (Fig. 1) produces an electric dipole suitable for sensing dielectric and resistive samples such as viruses and soot/dust particles.

To understand the operation of the MTM sensor and gain insight into its behavior at resonances, we simulated its electric-field (E-field) at 10 GHz with a vertically polarized E-field as shown in Fig. 2. At 10 GHz, the gap region has a large E-field that is necessary for sensitively detecting a sample that may be placed there.

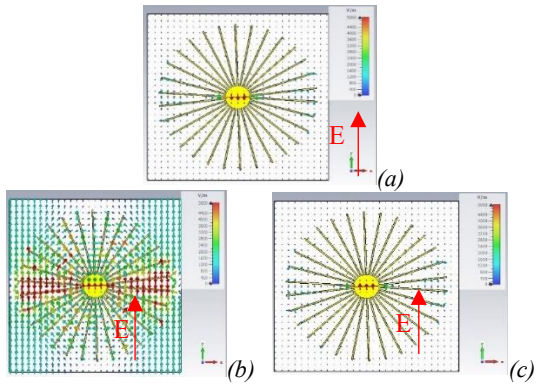

Fig. 2: E-field at 10GHz at different phase angles. (a) Phase=0° (b) Phase=90° (c) Phase=180°. Incident field was vertically polarized.

Other components of the E-fields in the sensor were also simulated and are shown in Fig. 3. The E-field is polarized along the Y axis and couples strongly with the vertical spokes setting up currents in them. The horizontal spokes, on the other hand, do not couple with the incident vertically polarized E-fields. The simulation shows that these horizontal spokes contribute to the capacitive central section (Fig. 3b). Microwave signals with arbitrary or random E-field polarizations are intercepted with spokes at corresponding angles in the sensor. The interaction between microwave signal and the sample (nanoparticles, saliva, etc.) is enhanced by the spoke structure and the electromagnetic properties of different materials in the gap (shown by Z_{sample} in Fig. 4) affect the MTM impedance differently enabling their detection through reflection coefficient measurements.

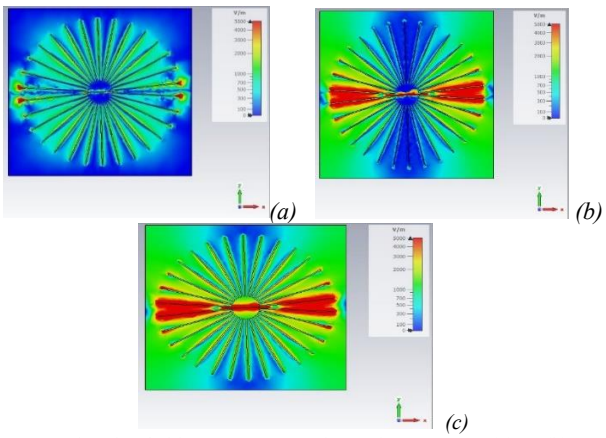

Fig. 3: Simulated E-field components in the spoke structure. (a) X (b) Y components and (c) combined E-field magnitude. Incident E was vertical (Y).

The spoke structure can be viewed as an electric dipole antenna. Near one of its resonances a simple lumped circuit model shown in Fig. 4 can be used to study its interactions with particles in the gap region. A non-magnetic sample in the gap region is modeled as an RC (red dotted) circuit as shown in Fig. 4. The sample interacts with the spoke structure through interfacial resistance (R_i) and capacitance (C_i). R_s in Fig. 4 is simply the resistance of the sample, while C_s is its capacitance calculated at the frequency of operation.

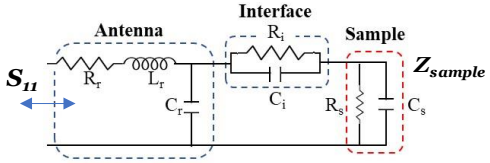

Fig. 4: A simplified equivalent circuit to model the interaction of a sample with R_s resistance C_s capacitance with through gap region of MTM sensor. The interfacial resistance and capacitance (R_i and C_i) electrically model the MTM-sample interaction.

The resonant MTM sensor is a complex structure with multiple resonances. Near 10 GHz, its behavior can be approximated by a simple 2nd order resonant system with resonant frequency $f_0 = 1/2\pi\sqrt{(L_r C_r)}$ while its impedance is $Z_r = R_r + j\omega L_r + 1/j\omega C_r$. Let's assume the impedance of the non-magnetic sample in Fig. 5 is $1/Z_s = 1/R_s + 1/j\omega Cs$. To estimate R_s and C_s of 1µL of water (approximately 1mm^3 volume), we consider the water droplet as a sphere with a radius 'r.' We then obtain the radius of the droplet by noticing that (4/3)*pi*r^3= 1mm^3 resulting in r=0.62 mm. The area covered by the droplet can also be estimated as $A = 4*pi*r^2 = 4.83$ mm^2. Noting that $C = \varepsilon_0\epsilon_r * (area/distance)$ and taking into account the average distance the gap of d=0.85 mm (this is larger than 0.004 mm of the split disk gap due to horizontal spokes), we calculate $C_{water} = 3.92\ pF$ and $C_{saliva} = 3.82\ pF$, or $\sqrt{\frac{C_{water}}{C_{saliva}}} = 1.01$, assuming that water sample has a relative permittivity of $\varepsilon_{water} \sim 78$ [3] and the saliva of a healthy human has a relative permittivity of $\varepsilon_{saliva} \sim 76$ [2]. We note that f_0 with water (f_{water}) or saliva (f_{saliva}) is indirectly proportional to the square root of the sensor's capacitance at resonance. The experimental frequencies for 1 1µL water and saliva were respectively 10.1762 GHz and 10.17172 GHz. Thus, $\frac{f_{saliva}}{f_{water}} = 1.004$. Instead of $\varepsilon_{saliva} \sim 76$ if we use ~ 76.6, $\frac{F_{saliva}}{F_{water}} = \sqrt{\frac{C_{water}}{C_{C_{saliva}}}} = 1.004$.

III. Experimental Results

Fig. 5 shows the experimental setup we used in our studies. An HP-8720C Vector Network Analyzer (VNA) and an X-band horn antenna were used to measure S_{11} of the MTM sensor situated directly under the horn. An absorbing foam under the MTM sensor was used to reduce reflection from the benchtop A data acquisition system collects all the measured data.

SARS-CoV-2 Samples: We placed 1 µL of different saliva samples in the sensor gap region (Fig. 6) and repeated our tests five times for each sample. 1 µl was easy to measure, and it was the smallest sample size with ~1000 viruses. The shift in S_{11} spectra in Fig. 7 is due to the slight difference between the dielectric constants of water and saliva. A healthy person's saliva has a relative average dielectric constant of ~76 [2], compared to water (~78) [3]. So, the saliva has lower capacitance compared to water. As a result, the resonance frequency increases for saliva samples. Fig. 8 shows the results of 5 different tests.

Infected and uninfected saliva were obtained through a collaborator in the University Hospitals as indicated in the acknowledgement. We maintain a biosafety level 2 facility in the laboratory for handling infected saliva samples. We used 1 uL saliva on the sensor that corresponds to the saliva particles emitted when we talk through our mouth cavity. We did not use any dilution solution. We used saliva directly obtained from COVID-19 patients in the hospital through our collaborator.

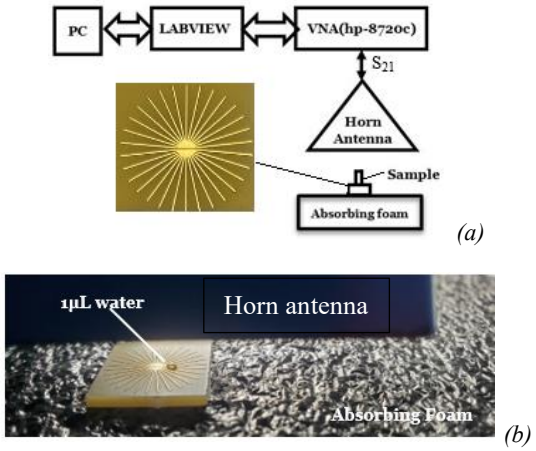

Fig. 5: a) Experimental setup used in our measurement. b) 1 µL deionized water sample placed on the spoke resonator under an X band horn antenna. VNA is the vector network analyzer.

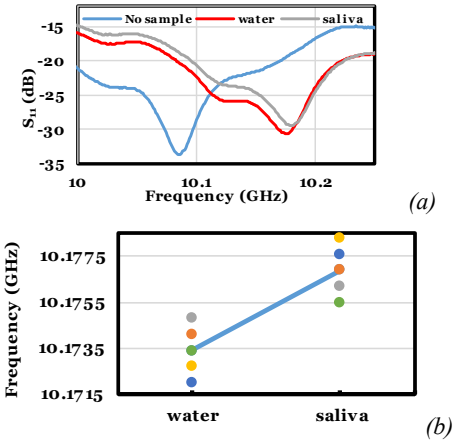

Fig. 6: a) S_{11} spectra for 1µL water and saliva sample placed in the gap. b) Frequency spread at resonance for 1µL of water and saliva samples.

Next, 1µL of SARS-COV-2 infected saliva were tested. When compared to the S_{11} responses of deionized water, and uninfected saliva, one can see a clear shift to the right in the resonance frequency (Fig. 7a). The frequency spread and average frequency response using 5 samples are shown are shown in Fig. 7b. The increase in resonance frequency indicates

a further decrease in the relative dielectric constant due to the presence of SARS COV-2 in the saliva. Both samples are 98-99 % water and the shift in the resonant frequency is expected to be relatively small. Infected saliva lowered the resonance frequency by ~1.1 MHz.

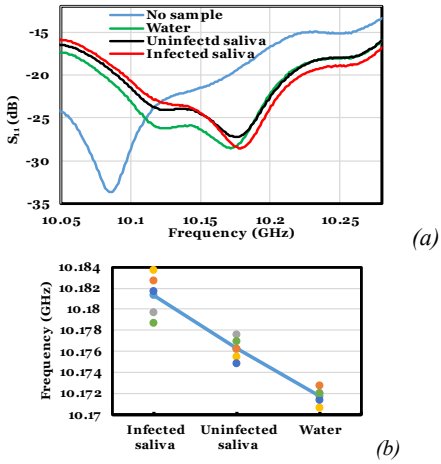

Fig. 7: S_{11} spectra of MTM sensor with 1μL water, uninfected saliva, and SARS-CoV-2 infected saliva. Resonance frequency of MTM sensor with 1μL SARS-CoV-2 infected saliva, uninfected saliva, and water droplets.

Dielectric Samples: In addition to aerosolized saliva particles, dust and soot particles also will deposit on the MTM sensors. These particulates are usually composed of carbon or silica and, in some cases, iron and other oxides and salts particles. The electromagnetic properties of these particles range from being purely dielectric in silica to semiconducting in soot to conducting and magnetic in iron and iron oxides. To study the sensitivity of MTM sensor in detecting the dielectric airborne particles we used a dielectric (duroid) sample with ε_r =5.84 and regular paper samples with ε_r ~ 1.8. The results for duroid samples are shown in Fig. 8. The resonance frequency decreases as we increased the gap's dielectric load till the dielectric sample becomes relatively large (~3x3 mm^2) affecting the Fabry-Perot resonances that set up between the horn antenna and the MTM sensor. The average sensitivity of the sensor for duroid was ~ 3.23 MHz/mm^3. Average sensitivity of the sensor for detecting paper was 1.06 MHz/mm^3.

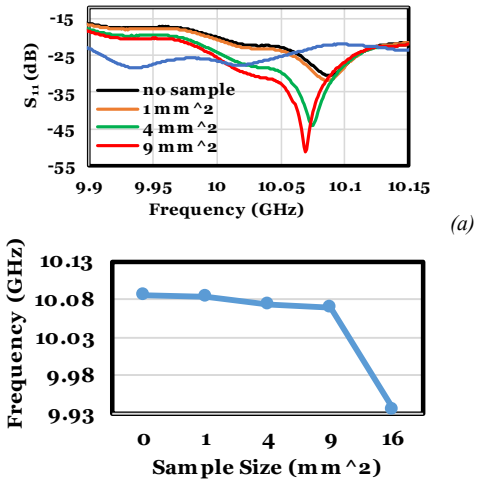

Fig. 8: a) S_{11} spectra and b) resonance frequency as a function of duroid samples with different sizes.

Iron Particles: S_{11} spectra with different lengths of a 1 mm diameter cylindrical iron samples with different lengths are shown in Fig. 9. The average sensitivity was 16.24 MHz/mm^3.

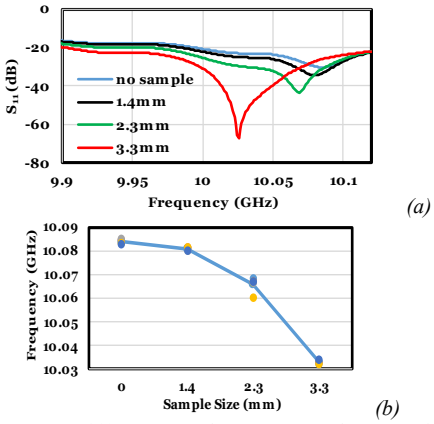

Fig. 9: a) S_{11} spectra and b) resonant frequency as a function of iron size.

Control Experiments with Uniform Substrates: We replaced the MTM sensor with a uniform dielectric substrate of the same dimension to perform control experiments shown in Fig. 10. Clearly, one cannot detect and differentiate various samples placed on the uniform substrate. These samples have dimensions much smaller than (<λ/30) the microwave wavelength of λ~3 cm at 10 GHz and with the MTM sensor structure, they can be detected.

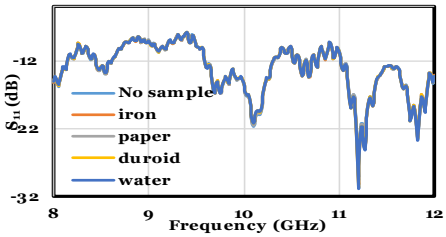

Fig. 10: S_{11} spectra for various samples placed on a dielectric substrate with ε_r=3.43. These samples are so small that the spectra are all on top of each other. However, when these samples were tested with the MTM sensor, they produced the results shown in this manuscript.

Tests with an array of MTM sensors: To cover large areas for environmental sensing, an array of MTM sensors is needed as schematically shown in Fig. 11. S_{11} spectra of each sensor were measured with and without 1 μL water droplet and are shown in Fig. 12. As expected, the shift in S_{11} frequency is largest when all four MTM sensors had water droplets. The location of the MTM sensor in the array also affected its S_{11} spectrum and can be used for multiplexing.

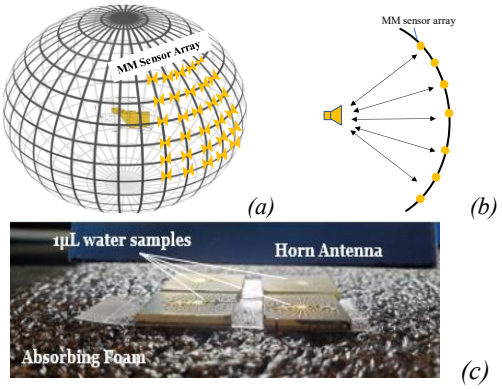

Fig. 11: a) and b) MTM sensor arrays can be located over large areas to monitor airborne viral and other particles [43]. c) Experimental setup with 4 MTM sensors to investigate feasibility of large area sensing with MTM sensors.

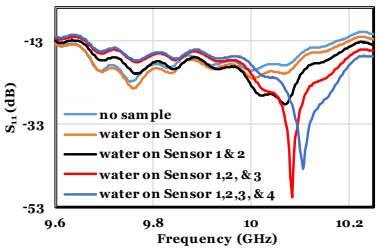

Fig. 12: S_{11} spectra for 4 MTM sensor array with and without 1 μL deionized water droplets.

IV. Sensitivity Analysis

In our measurements we used the resonance frequency of the MTM structure near f_0=10 GHz as the sensor signal. We measured f_0 with different amounts of materials and calculated the sensor's sensitivity. The sensitivity (S) is given by: $S=\Delta f/d$, where d is the physical dimension or volume of the material and Δf is the change in the sensor resonance frequency. We rely on calibration curves (f_0 *versus the amount of material*) to quantify the amount of substance that is detected by the sensor. Table I shows a comparison between the sensitivity of our sensor and other reported sensors. It is important to note that the sensor specificity in this work is provided by the ~10 GHz electromagnetic properties of the SARS-CoV-2 viral particles that are different than other particles we examined. For more specificity, the sensor surface can be coated with aptamers designed to bind with the spiking proteins of the SARS-CoV-2 viral particles [8,25].

Table I: Comparison between some recent SARS COV-2 detection methods and the MTM microwave method discussed here.

Year	2021 [10]	2021 [15]	2021 [16]	2022 This work
Detection Method	Chemical	Electrochemical	Terahertz plasmonic meta sensor	Microwave sensor
Sensitivity	1ng/mL SARS-CoV-2 antibodies	0.074 fg/mL of saliva	4.2 fM spike proteins	94.6MHz/1μL of saliva
Detection time	30 minutes	100ms	80 minutes	Real time

V. Conclusion

We demonstrated the ability of MTM sensors in detecting small amounts of materials and objects (<λ/30) using X-band microwave signals. We showed that it has good sensitivity in detecting SARS-COV-2 infected and uninfected human saliva of 94.6MHz/1μL and 89.5 MHz/1μL respectively. For dielectric samples (duroid) the sensitivity was ~3.23 MHz/mm^3 and for metallic samples was ~ 16.25 MHz/ mm^3. We also demonstrated the feasibility of forming an MTM sensor array and interrogating them for applications in sensing particles spread over large surfaces. The data presented here show the feasibility of using an MTM-based SARS-CoV-2 sensor. More work needs to be carried out to develop a turn-key remote SARS-CoV-2 sensor.

Acknowledgment

This work was supported by a RAPID grant from NSF (#2030359), a grant from EXAMIN, LLC and by the USTAR Program. Infected salivae were obtained from Dr. Elizabeth Middleton of Department of Internal Medicine, University of Utah. SARS-CoV-2 sensors partially discussed here are being commercialized by the University of Utah. Please contact Dr Aaron Duffy (aaron.duffy@utah.edu) for more information.

References

[1] Schumann Guy J.-P., "Grand Challenges in Microwave Remote Sensing." Frontiers in Remote Sensing." Vol. 1, Frontiers in Sensing (2020). doi=10.3389/frsen.2020.603650

[2] U. R. L. D. J. Shinde and S. C. Mehrotra, "Signal Processing as a Probe to Study Dielectric Properties of Mouth Cancer Patient's Saliva," vol. 4, no. 4, pp. 1483–1485, 2013.

[3] J. L. Aragones, L. G. Macdowell, and C. Vega, "Dielectric Constant of Ices and Water: A Lesson about Water Interactions," J. Phys. Chem. A, vol. 115, pp. 5745–5758, 2011, doi: 10.1021/jp105975c.

[4] Y. Zhang, J. Zheng, J. Yu, and H. He, "Mechanical characterization of in vitro-formed short-term salivary pellicle," Journal of Biomechanics, vol. 66. pp. 194–197, 2018, doi: 10.1016/j.jbiomech.2017.11.001.

[5] Bar-On YM, Flamholz A, Phillips R, Milo R. SARS-CoV-2 (COVID-19) by the numbers. Elife. 2020;9:e57309. Published 2020 Apr 2. doi:10.7554/eLife.57309.

[6] R. I. MacCuspie, N. Nuraje, S. Y. Lee, A. Runge, and H. Matsui, "Comparison of electrical properties of viruses studied by AC capacitance scanning probe microscopy," Journal of the American Chemical Society, vol. 130, no. 3. pp. 887–891, 2008, doi: 10.1021/ja075244z.

[7] Massood Tabib-Azar, Shaun McKellar, Cynthia Furse, "Free Space Resonant Electromagnetic Sensing Techniques to Detect Airborne Viral and Environmental Particles Using Atomic Layer Graphene." NT21: International Conference on the Science and Application of Nanotubes and Low-Dimensional Materials. Proceeding, p. 65 (2021).

[8] Massood Tabib-Azar, "Electronic Spiking Protein-Based COVID Sensors." 2021 Meet. Abstr. MA2021-01 2036. https://iopscience.iop.org/article/10.1149/MA2021015220 36mtgabs/meta

[9] Massood Tabib-Azar and Elizabeth Middleton, " Electronic Sensors to Detect COVID-19 Viruses in Real-Time." Submitted for publication 10/22/2021.

[10] P. K. Dave, R. Rojas-Cessa, Z. Dong, and V. Umpaichitra, "Survey of saliva components and virus sensors for prevention of SARS-COV-2 and infectious diseases," Biosensors, vol. 11, no. 1, 2021, doi: 10.3390/bios11010014.

[11] A. Samavati et al., "Sustainable and fast saliva-based SARS-COV-2 virus diagnosis kit using a novel GO-decorated Au/FBG sensor," Chem. Eng. J., vol. 420, no. P2, p. 127655, 2021, doi: 10.1016/j.cej.2020.127655.

[12] L. Xu, D. Li, S. Ramadan, Y. Li, and N. Klein, "Facile biosensors for rapid detection of SARS-COV-2," Biosens. Bioelectron., vol. 170, no. August, p. 112673, 2020, doi: 10.1016/j.bios.2020.112673.

[13] A. Yakoh, U. Pimpitak, S. Rengpipat, N. Hirankarn, O. Chailapakul, and S. Chaiyo, "Paper-based electrochemical biosensor for diagnosing SARS-COV-2: Detection of SARS-CoV-2 antibodies and antigen," Biosens. Bioelectron., vol. 176, no. November 2020, p. 112912, 2021, doi: 10.1016/j.bios.2020.112912.

[14] Sharma S, Saini S, Khangembam M, Singh V (2021) Nanomaterials-based biosensors for COVID-19 detection—a review. IEEE Sens J 21:5598–5611. https://doi.org/10.1109/JSEN.2020.3036748

[15] B. Shan et al., "Multiplexed Nanomaterial-Based Sensor Array for Detection of SARS-COV-2 in Exhaled Breath," ACS Nano, vol. 14, no. 9, pp. 12125–12132, 2020, doi: 10.1021/acsnano.0c05657.

[16] E. Saatçi and S. Natarajan, "State-of-the-art colloidal particles and unique interfaces-based SARS-CoV-2 detection methods and SARS-COV-2 diagnosis," Curr. Opin. Colloid Interface Sci., vol. 55, p. 101469, 2021, doi: 10.1016/j.cocis.2021.101469.

[17] K. Wu et al., "Magnetic-nanosensor-based virus and pathogen detection strategies before and during SARS-CoV-2," ACS Appl. Nano Mater., vol. 3, no. 10, pp. 9560–9580, 2020, doi: 10.1021/acsanm.0c02048.

[18] A. Ramanujam, S. Almodovar, and G. G. Botte, "Ultra-fast electrochemical sensor for point-of-care SARS-CoV-2 diagnosis using non-invasive saliva sampling," Processes, vol. 9, no. 7, 2021, doi:

10.3390/pr9071236.
[19] A. Ahmadivand, B. Gerislioglu, Z. Ramezani, A. Kaushik, P. Manickam, and S. A. Ghoreishi, "Functionalized terahertz plasmonic metasensors: Femtomolar-level detection of SARS-CoV-2 spike proteins," Biosens. Bioelectron., vol. 177, no. June 2020, p. 112971, 2021, doi: 10.1016/j.bios.2021.112971.
[20] Das, Chandreyee Manas et al. "Gold Nanorod Assisted Enhanced Plasmonic Detection Scheme of COVID-19 SARS-CoV-2 Spike Protein." Advanced theory and simulations vol. 3,11 (2020): 2000185. doi:10.1002/adts.202000185
[21] Cennamo, Nunzio, D'Agostino, Girolamo, Perri, Chiara, Arcadio, Francesco, Chiaretti, Guido, Parisio, Eva Maria, Camarlinghi, Giulio, Vettori, Chiara, Di Marzo, Francesco, Cennamo, Rosario, Porto, Giovanni, Zeni, Luigi, "Proof of Concept for a Quick and Highly Sensitive On-Site Detection of SARS-CoV-2 by Plasmonic Optical Fibers and Molecularly Imprinted Polymers." Sensors 21 (5), 1681 (2021). doi: 10.3390/s21051681
[22] Ahmadivand A, Gerislioglu B, Ramezani Z, Kaushik A, Manickam P, Ghoreishi SA. Functionalized terahertz plasmonic metasensors: Femtomolar-level detection of SARS-CoV-2 spike proteins. Biosens Bioelectron. 2021;177:112971. doi:10.1016/j.bios.2021.11297.
[23] Lee SH, Lee YK, Lee SH, Kwak J, Song HS, Seo M. Detection and discrimination of SARS-CoV-2 spike protein-derived peptides using THz metamaterials. Biosens Bioelectron. 2022 Apr 15;202:113981. doi: 10.1016/j.bios.2022.113981. Epub 2022 Jan.
[24] Kadic, M., Milton, G.W., van Hecke, M. et al. 3D metamaterials. Nat Rev Phys 1, 198–210 (2019). https://doi.org/10.1038/s42254-018-0018-y.
[25] W. Xu, L. Xie and Y. Ying, "Mechanisms and applications of terahertz metamaterial sensing: a review." Nanoscale, 2017, 9, 13864-13878. DOI: 10.1039/C7NR03824K.

Massood Tabib-Azar received M.S. and Ph.D. degrees in electrical engineering from the Rensselaer Polytechnic Institute in 1984 and 1986, respectively. In 1987 he joined the faculty of EECS department at Case Western Reserve University. He was a fellow at NASA during 1992-1992, on Sabbatical at Harvard University during 93-94, at Yale University during 2000-2001, at UC Berkeley during 2015-16, and at the Massachusetts Institute of Technology in 2016. He was a Program Director at the ECCS Division of National Science Foundation during 2012-2013 Academic Year. Massood is currently a USTAR Professor of ECE at the University of Utah, Electrical and Computer Eng. Department with an adjunct appointment in Bioengineering Department. His current research interests include nanometrology, micro-plasma devices, nano-electromechanical computers, novel devices based on solid electrolytes (memristors), sensors and actuators, injectable bio-systems, quantum sensing, and quantum computing. His teaching interests include development of courses in electronic device physics and electromagnetics with an emphasis on solving problems and the use of computer-aided instruction tools. He is author of three books, two book chapters, more than 260 journal publications, and numerous conference proceeding articles. He has introduced and chairs many international symposia in his fields of interest. He is in the Editorial Board of IEEE Electron Device Letters.

Dr. Tabib-Azar is a recipient of the 1991 Lilly Foundation Fellowship and he is a member of the New York Academy of Sciences, IEEE (Electron Devices), APS, AAPT, and Sigma Xi research societies. He has also received more than 14 certificate of appreciation and recognition for his professional activities and a best paper award from Design Automation conference in 2001 for his work on electromagnetic properties of interconnects and defects in ICs, a best paper award from International Conference on Intelligent Robots and Systems in 2004 for his work on Human-Machine Interface, and a best paper award from ISQED for his work on NEMS Processors in 2011.

Mohammad Ashif Hossain Chowdhury received his BS degree in electrical and electronic engineering from Chittagong University of Engineering and Technology, and MS degree in electrical engineering from the University of Texas Rio Grande Valley in 2017 and 2021, respectively. Currently he is pursuing PhD in ECE at the University of Utah. Before starting his MS, he had worked as an engineer at the Bangladesh Atomic Energy Commission during 2017-2019. His research interests include applied electromagnetics, sensors, optics and photonics.